Causes of Changes in the Denmark Strait Overflow

Armin Köhl, Rolf H. Käse, and Detlef Stammer

Institut für Meereskunde Zentrum für Meeres- und Klimaforschung, Universität Hamburg, Hamburg, Germany

Nuno Serra

Instituto de Oceanografia, Faculdade de Ciências da Universidade de Lisboa, Lisbon, Portugal

ABSTRACT

The warming Nordic seas potentially tend to decrease the overflow across the Greenland–Iceland–Scotland Ridge (GISR) system. Recent observations by Macrander et al. document a significant drop in the intensity of outflowing Denmark Strait Overflow Water of more than 20% over 3 yr and a simultaneous increase in the temperature of the bottom layers of more than 0.4°C. A simulation of the exchange across the GISR with a regional ocean circulation model is used here to identify possible mechanisms that control changes in the Denmark Strait overflow and its relations to changed forcing condition. On seasonal and longer time scales, the authors establish links of the overflow anomalies to a decreasing capacity of the dense water reservoir caused by a change of circulation pattern north of the sill. On annual and shorter time scales, the wind stress curl around Iceland determines the barotropic circulation around the island and thus the barotropic flow through Denmark Strait. For the overlapping time scales, the barotropic and overflow component interactively determine transport variations. Last, a relation between sea surface height and reservoir height changes upstream of the sill is used to predict the overflow variability from altimeter data. Estimated changes are in agreement with other recent transport estimates based on current-meter arrays.

1. Introduction

The Denmark Strait sill acts as a key region for the global ocean circulation: dense water that is being formed in the Nordic seas has to enter the North Atlantic Ocean through the strait and plays subsequently an important role in setting the strength of the meridional overturning circulation and in the formation of the characteristics of North Atlantic Deep Water (NADW). Moreover, as demonstrated by Kösters et al. (2005) in a coupled model study, the strength of the flow over the Denmark Strait sill impacts the European climate. Understanding variability in the exchange between the Nordic seas and the Atlantic is therefore of fundamental importance for understanding modifications of the climate over Europe.

A steady state in the outflow of dense water from the Nordic seas into the North Atlantic requires a balance between production of dense water and outflow. If this long-term balance is disturbed (e.g., through changing buoyancy forces in the Nordic seas or through enhanced land ice melting) changes must occur in the water mass formation in the Nordic seas, in the exchange of waters between the North Atlantic and the Nordic seas, and presumably in the climate over northern Europe. Although on short time scales the Denmark Strait overflow (DSO) is pulsating because of plume instability (Girton et al. 2001; Swaters 1991), there was a general understanding (Dickson and Brown 1994; Saunders 2001) that its strength to first order is not changing on time scales longer than a few months. However, Bacon (1998) has presented a decrease of the deep western boundary current downstream of the overflows since the early 1980s, which he related to the Arctic warming. Moreover, recent observations (Macrander et al. 2005) document a significant drop in the intensity of outflowing Denmark Strait Overflow Water (DSOW) of more than 20% over 3 yr and a simultaneous increase in the temperature of the bottom layers of more than 0.4°C. Based on this observational evidence, the notion of a static outflow from the Nordic

Corresponding author address: Armin Köhl, Institut für Meereskunde Zentrum für Meeres- und Klimaforschung, Universität Hamburg, Bundesstr. 53, 20146 Hamburg, Germany.
E-mail: armin.koehl@zmaw.de

seas to the Atlantic has changed. Yet, a dynamic explanation of observed changes and its underlying causes is still missing.

Käse and Oschlies (2000) demonstrated that the strength of the DSO to first order is in hydraulic balance. Whitehead (1998) considered hydraulic transport limitations and showed that for a wide sill, the pressure force drives the drainage of the Nordic seas and the transport is proportional to the square of the height difference between upstream dense water level and sill depth and linearly depending on the density difference. According to the theoretical considerations, a 20% anomaly in the Denmark Strait outflow observed by Macrander et al. (2005) can be achieved either by a 20% change in the cross-sill density gradient or by only a 9.5% change in reservoir height of dense water upstream of the sill. Recent changes in the DSO strengths occurred on short time scales on which significant density changes are less likely. To understand those changes it seems therefore plausible to investigate, in particular, causes that lead to changes in reservoir height.

A respective approach was also followed recently by Hansen et al. (2001) who hindcasted a decrease of the outflow through the Faroe Bank Channel (FBC), the other major channel of the Greenland–Iceland–Scotland Ridge (GISR) from the reservoir height at a location in the Norwegian Sea. They found a decrease of at least 20% from 1950 to 1999. A critical assessment of this approach considering upstream basin potential vorticity was given by Helfrich and Pratt (2003). In the present context it is also noteworthy that the trend diagnosed by the authors reversed at the time their paper was published (B. Hansen 2004, personal communication). The simultaneous weakening of the DSO [observed in 2001 by Macrander et al. (2005)] suggests that both outflows of dense water from the Nordic seas are coupled but anticorrelated in the sense that anomalies occur with opposite phase on either side of Iceland but that the net outflow across the GISR approximately stays constant.

Østerhus et al. (2005) observed that since the mid-1990s the inflow of warm and saline Atlantic water, crossing the GISR on either side of Iceland toward the Arctic, does vary in time such that the inflow through Faroe–Shetland Channel seems to be anticorrelated with that of the other two branches east and west of Iceland and does not show a clear seasonal cycle. According to their measurements, the time-mean Atlantic inflow during the period 1999 through 2001 was 8.5 Sv (1 Sv $\equiv 10^6$ m^3 s^{-1}), 0.313 PW, and 303 $\times$ 10^6 kg s^{-1} in terms of volume, heat (relative to 0°C), and freshwater flux, respectively. During the same period, the aver-aged temperature and salinity of the Atlantic inflow was 8.5°C and 35.25 psu, respectively.

Observed out-of-phase changes of the flow field north and south of Iceland (near the surface and at depth) appear consistent with results from Biastoch et al. (2003) who suggested that the barotropic gyre circulation, encompassing the subpolar North Atlantic and the Greenland–Iceland–Norwegian (GIN) Seas, modulates the throughflow such that an increasing cyclonic gyre enhances the DSO while decreasing the outflow through FBC. Nilsen et al. (2003) found the same relation of the transports east and west of Iceland from their model studies.

Until recently it was assumed that the water reaching the Denmark Strait was fed exclusively through the East Greenland Current (EGC; Strass et al. 1993; Fahrbach et al. 2002; Mauritzen 1996a,b). However, Jónsson and Valdimarsson (2004) argue that the DSOW is carried to the sill not only by the EGC but also by a hitherto not reported ocean current that runs along the Icelandic slope. The authors describe the current as a narrow subsurface jet with measured speeds exceeding 40 cm s^{-1}. No seasonal cycle in the current could be revealed from the observations because of the limited length of the time series, which seems consistent with the notion that no seasonal cycle can be identified in the DSOW from measurements (Dickson et al. 1999).

In the following, we will revisit the question of the dynamic causes for recently observed changes in the DSO (Macrander et al. 2005) using results of a numerical simulation of the flow field in the eastern subpolar North Atlantic and the Nordic seas. According to the nature of the changes, our focus here will be on time scales of up to a decade and on variations of the reservoir height as a primary cause for changes in DSO variations. A multiple regression analysis will show that the decrease in DSO and associated changes in reservoir height can be related to changes in the wind stress curl around Iceland.

As explained in more detail below, the study is based on a model simulation that is driven with the atmospheric state of 1992–2003 and is supposed to simulate the circulation during this period. However, two shortcomings have to be pointed out that concern changes simulated by the model. First, boundary conditions are taken from a global 1° state estimation that assimilated only limited data in the Nordic seas and was closed to the Arctic. The realism of the northern boundary conditions with respect to observed changes is therefore limited. Second, because of the dependence of the circulation on the boundary conditions there is no spinup (which would require boundary conditions before the 1990s) previous to the simulation. Therefore, the simu-

lated circulation changes also reflect small (but unspecified) adjustment processes. After a presentation of the numerical model in the following section, we present in section 3 characteristics of the modeled circulation with a focus on the sources of the DSO. In section 4 we discuss mechanisms that describe DSO variability, and in section 5 we discuss their observability. The concluding remarks follow in section 6.

2. The model

Our numerical simulations are based on the Massachusetts Institute of Technology (MIT) ocean general circulation model (Marshall et al. 1997a,b), which was implemented for the GISR region and covers the eastern subpolar North Atlantic and Nordic seas from 51° to 78°N. The realistic bottom topography is based on the ETOPO2 dataset, which in our model domain is identical to the Smith and Sandwell (1997) topography. The horizontal grid is isotropic with a zonal resolution of 0.1°. The thickness of 30 vertical levels varies from 10 m near the surface to 500 m at depths. Around the sill depths of the GISR passages layer thicknesses are smaller than 100 m. To enhance the realism of the results, the model is nested into the global 1° state estimation of the Estimating the Circulation and Climate of the Ocean (ECCO) consortium (Stammer et al. 2002) that was constrained by most available ocean data (see Köhl et al. 2007 for details). The nesting was accomplished by specifying monthly mean ECCO values of temperature, salinity, and velocity at the open boundaries, which is complemented by a relaxation of the model's field toward ECCO monthly mean velocity fields over an inner domain of 10 grid points (see Zhang and Marotzke 1999 for details). The net transport through the boundaries from the 1° model was adjusted to allow 2 Sv of transport exiting into the Barents Sea and 1 Sv entering through Fram Strait. The transport through the western boundary was enhanced by 1 Sv to close the volume budget. The model was started from rest and Levitus and Boyer (1994)/Levitus et al. (1994) temperature and salinity in 1992. Over the period 1992 to 2003 the simulation was forced by the daily atmospheric state obtained from the National Centers for Environmental Prediction–National Center for Atmospheric Research (NCEP–NCAR) reanalysis project. Surface fluxes of heat, freshwater, and momentum (wind stress) were calculated from the atmospheric and model variables using bulk formula according to Large and Pond (1981, 1982). The vertical profile of absorption of shortwave heat flux is modeled by the analytical formula of Paulson and Simpson (1977) for time-dependent ocean water types (ranging from Ia in winter

to II in summer) after Jerlov (1968). The model formulation includes a parameterization for vertical mixing by the K-profile parameterization scheme of Large et al. (1994) and a dynamic/thermodynamic sea ice model of Zhang and Rothrock (2000). Background coefficients of vertical diffusion and viscosity are 10^{-6} and 10^{-4} m^2 s^{-1}, respectively. Horizontally, biharmonic diffusion and viscosity represent unresolved eddy mixing. Coefficients of horizontal diffusion and viscosity are both 10^{10} m^4 s^{-1}.

3. Simulated and observed transport variations

Figure 1 shows an instantaneous field of the simulated sea surface temperature (SST) over the model domain for May 2003 together with simultaneous SST field, observed by the Advanced Microwave Scanning Radiometer for the Earth Observing System (AMSR-E) microwave sensor on board of the National Aeronautics and Space Administration (NASA) Earth Observing System (EOS) *Aqua* platform (Wentz et al. 2000). On the eddy scales, the model SST shows substantial finescale structures that were smoothed out in the observations because of their coarse spatial resolution of about 50 km. On larger scales, however, the model field agrees reasonably well with the observations both in temperature amplitudes and structures. As an example, the position of the simulated 1°C isotherm, which marks the location of the Arctic Front, overall matches the observations. However, its observed southeastward excursion east of Iceland is less pronounced in the simulation. This can be interpreted as the result of a weaker East Icelandic Current in the model during that year, although the current appears to be stronger during other years. We note that on the seasonal cycle, the model SST is substantially biased toward warmer temperatures in summer and early autumn and only slightly toward colder temperatures in winter and spring (not shown). To a large extent, this bias can be explained by the underestimation of the late summer mixed-layer depths, which is probably caused by too strong an absorption of shortwave radiation associated with Jerlov water type II during late summer. Using water type Ia or Ib removes this bias.

Figure 2 shows a schematic of time-mean transports across the GISR split into light inflow and dense outflow. Here and in the following, the dense outflow is specified as water denser than $\sigma_0 = 27.8$. The exchange can be characterized accordingly by water lighter than 27.8, or, alternatively, using the classic definition of Atlantic Water characterized by salinity values above 35.0 psu. For light water east of Iceland, transport values in the two classes of definitions agree well with each other,
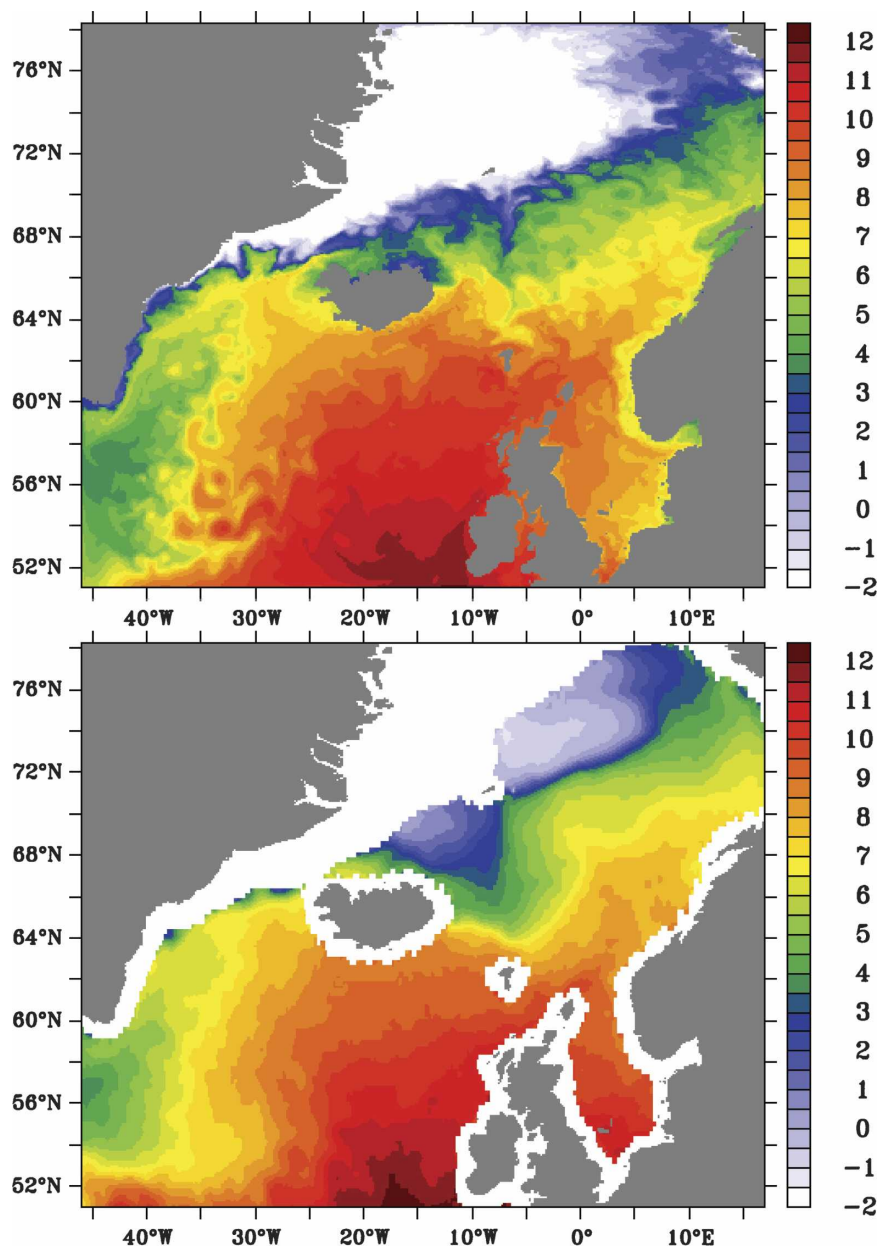
FIG. 1. Sea surface temperature (°C) during May 2003 (top) as simulated by the model and (bottom) as observed by the AMSR-E instrument on board the EOS *Aqua* platform. The Arctic front, characterized by temperatures between about 0° and 2°C, is marked by dark blue colors. White areas represent ice-covered regions in the model in the top panel. In the bottom panel, white areas represent regions with land- or ice-contaminated SST observations. Contour increment is 0.5°C in both panels.

but volume, heat, and salt transports are about one-third lower than those estimated by Østerhus et al. (2005) from observations. West of Iceland, however, transport values for the light water differ considerably depending on its definition, whether it is density or salinity based. There, the northward inflow of 1.2-Sv Atlantic water with salinity exceeding 35.0 psu is bal-

anced by an almost equal amount of freshwater (less than 35.0 psu) that flows southward. The net transport above $\sigma_0 = 27.8$ is thus close to zero. Volume, heat, and salt fluxes of Atlantic water estimated by Østerhus et al. (2005) based on the salinity criteria are one-third lower than the modeled transports.

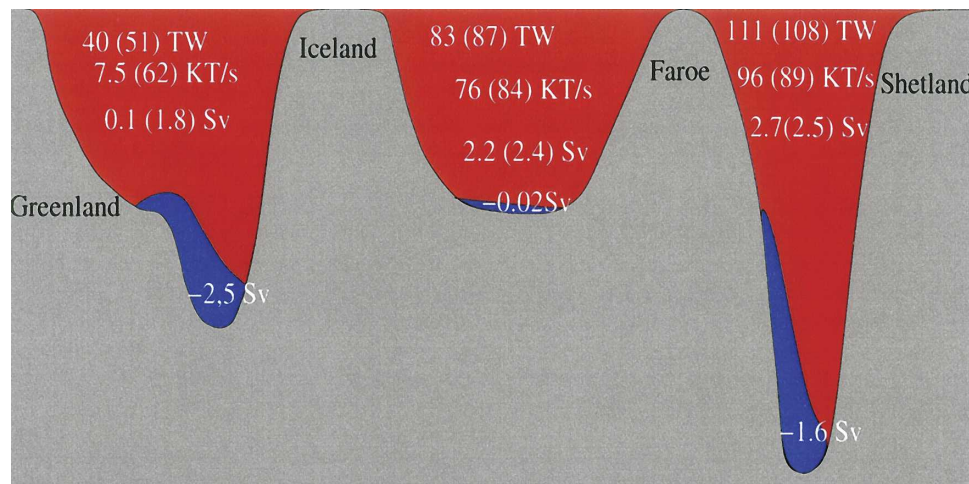The mean DSO of 2.4 Sv is low, but within error bars

FIG. 2. Schematic of volume, salt, and heat transport across the GISR. The heat transport is relative to 0°C. The values are provided for the density classes above and below the density surface $\sigma_0 = 27.8$. Values in parentheses represent water masses with salinity larger or smaller than 35.0 psu. All numbers represent time-mean values of the transports calculated from individual 3-day snapshots and include eddy transports.

of the estimate provided by Girton et al. (2001) (2.7 Sv) who suggested that the classical transport estimates based on temperature criteria (see Dickson and Brown 1994) describe (because of different sampling strategies) only some fraction of an otherwise larger transport value. Macrander et al. (2005) reported an overflow time series from 1999 onward with higher values of 3.0–3.7 Sv. However, we note that our model transports are calculated from meridional sections along 25°W, which lie 2° east of the mooring sites of Macrander et al. (2005) or Girton et al. (2001). This section was chosen because transport values remain invariant over the range 25°–20°W, whereas the transport increases by about 0.3 Sv from 25° to 27°W as a result of entrainment. It is unknown, however, if this also holds for the real ocean. The dense ($\sigma_0 < 27.8$) overflow through the Faroe–Shetland Channel (FBO) with 1.6 Sv is also lower in amplitude than observed values ranging from 2 (Borenäs and Lundberg 2004) to 2.5 Sv (Mauritzen et al. 2005).

Table 1 summarizes amplitude and phase of the seasonal cycle, as well as the linear trend computed over the 12-yr period of volume, salt, and heat flux relative to 0°C. In the density class $\sigma_0 < 27.8$ the amplitude of the seasonal cycle of volume and salt transports are similar for the Greenland–Iceland and Faroe–Shetland sides and lie around 0.6 Sv and $21 \times 10^6 \text{ s}^{-1}$. The phase indicates anticorrelation between those transports. The transport trends over the 12 yr are small except for the Greenland–Iceland salt transport that amounts to about the same size as the mean transport. Using the

above density as water mass boundary, the corresponding seasonal cycle is much larger than the mean transport but less than 20% if the salinity criterion is used. This is not surprising since only the salinity-based criterion describes the inflow, whereas the density-based definition of the transports leads to a combination of shallow inflow and outflow. The seasonal cycle of the volume transport for the density class $\sigma_0 > 27.8$ shows that the exchange of dense water between Iceland and Faroe is dominated by fluctuations. It also shows a significant seasonal contribution (with 0.6 Sv, 30% of the mean) for the Shetland Channel but much smaller fraction for the western side of Iceland.

The time-mean circulation of the dense water layer in the source region of the DSOW, northwest of Iceland, is shown in Fig. 3a as an average for the years 1993–96, which describes a specific state of the circulation as described below. The figure displays the vertically integrated flow field from the depth range below the $\sigma_0 = 27.8$ isopycnal. Highest transport density values are associated with the DSO. From the figure it is obvious that two current branches feed the DSO, one following the Greenland shelf slope, the other one following the Iceland slope. The vertical structure of both is displayed in Fig. 3b showing a meridional section along 20.5°W of the zonal velocity component with superimposed isopycnals near the entrance of the Denmark Strait north of the sill. The figure shows the shallow Atlantic inflow at 67.5°N and the vertical structure of the two westward flowing branches. The southern branch reveals a structure similar to the one recently

TABLE 1. The table summarizes amplitude and phase of the seasonal cycle, and the trend of volume, salt, and heat transport relative to 0°C. Values are shown for the three segments across the GISR displayed in Fig. 2. Values of the alternative definition using salinity classes above 35.0 psu are in parentheses. Units are as follows: $Sv = 10^6$ m^3 s^{-1}, $TW = 10^{12}$ W, kt $s^{-1} = 10^6$ kg s^{-1}.

	Greenland–Iceland	Iceland–Faroe	Faroe–Shetland
Density class $\sigma_0 < 27.8$ (salinity above 35.0 psu)			
Volume			
Amplitude	0.632 (0.182) Sv	0.115 (0.113) Sv	0.59 (0.6) Sv
Phase	211.378 (55.008) days	51.272 (52.28) days	14.814 (17.232) days
Trend	0.015 (0.018) Sv yr^{-1}	−0.072 (−0.082) Sv yr^{-1}	0.003 (0.007) Sv yr^{-1}
Salt			
Amplitude	21.745 (6.405) kt s^{-1}	4.043 (3.962) kt s^{-1}	20.846 (21.166) kt s^{-1}
Phase	212.154 (55.059) days	51.318 (52.35) days	14.808 (17.208) days
Trend	0.524 (0.64) kt s^{-1} yr^{-1}	−2.536 (−2.879) kt s^{-1} yr^{-1}	0.113 (0.264) kt s^{-1} yr^{-1}
Heat			
Amplitude	1.42 (0.943) TW	1.92 (1.85) TW	4.848 (4.845) TW
Phase	239.149 (21.829) days	34.845 (32.03) days	354.287 (355.24) days
Trend	0.093 (0.284) TW yr^{-1}	0.18 (0.194) TW yr^{-1}	0.147 (0.162) TW yr^{-1}
Density class $\sigma_0 > 27.8$			
Volume			
Amplitude	0.155 Sv	0.184 Sv	0.6 Sv
Phase	219.909 days	222.293 days	17.232 days
Trend	0.04 Sv yr^{-1}	−0.073 Sv yr^{-1}	0.007 Sv yr^{-1}

observed by Jónsson and Valdimarsson (2004) at 22°W. In the model the current starts to widen significantly west of 21°W; at 20.5°W, its core can be found between 400- and 600-m depth with maximum velocity amplitudes of typically 10 cm s^{-1} near the bottom. Dense water (see the $\sigma_0 = 28.08$ isopycnal) domes up near the Icelandic continental slope and forms a sharp front there. In contrast to the southern branch, the northern branch, which is a continuation of the EGC, is surface intensified and shows also a substantial fraction of the transport on the Greenland shelf with densities $\sigma_0 < 27.8$.

Time series of the transport of both branches feeding the DSO with density $\sigma_0 > 27.8$ are shown in Fig. 4. The current northwest of Iceland shows considerable variability in the range of values 0.5–1.5 Sv. This has to be compared with 0.5–2.5 Sv for the total transport of the jet (including lighter water; not shown). Jónsson and Valdimarsson (2004) observed values of 0.6 and 2.7 Sv during a short period in November 2001 and 2002, respectively, while in the model the time-mean total November transports are about 1.8 Sv for both years. Because of the substantial transport variability within a month (order of 2 Sv), the representativeness of Jónsson's and Valdimarsson's values observed by acoustic Doppler current profilers (ADCPs) during a 4-day period has to be questioned. It seems obvious that long time series are required to gain stable information about currents and long-period transport changes.

We note that the variability of the southern and northern branches are anticorrelated. While during the first and last three years both branches flux an equal amount of volume westward, after 1994 the transport of the EGC increases by more than 0.5 Sv; it decreases again after 1999 but does not return to the previous strength. The total volume of dense water flowing toward the Denmark Strait shows less long-period variability than seen in each branch alone.

In its lower panel, the figure shows time series of the transport for water with density higher than $\sigma_0 = 27.8$ crossing the Denmark Strait and the Faroe Bank Channel. Also shown in the figure is the net southward transport of dense water through both passages. A similar picture as before for the two branches east of Iceland emerges. Both time series are negatively correlated with $r = 0.53$ as suggested previously by Biastoch et al. (2003). Between 1994 and 1999, the DSO increases while the FBO decreases by the same amount; after 1999 the trend reverses and the DSO decreases, which is consistent with the findings of Hansen et al. (2001) that we described in the introduction. The intensification of the EGC therefore coincides with the intensification of the DSO.

Figure 5 shows the separation of the Denmark Strait volume transports in the dense ($\sigma_0 > 27.8$) and light part ($\sigma_0 > 27.8$) together with the total barotropic transport. A clear correspondence of dense overflow and barotropic transport ($r = 0.85$) on all time scales considered here suggests that most of the observed variations in the overflow is related to changes in the barotropic transport. However, it is seen that the deep outflow has less variability than the barotropic trans-
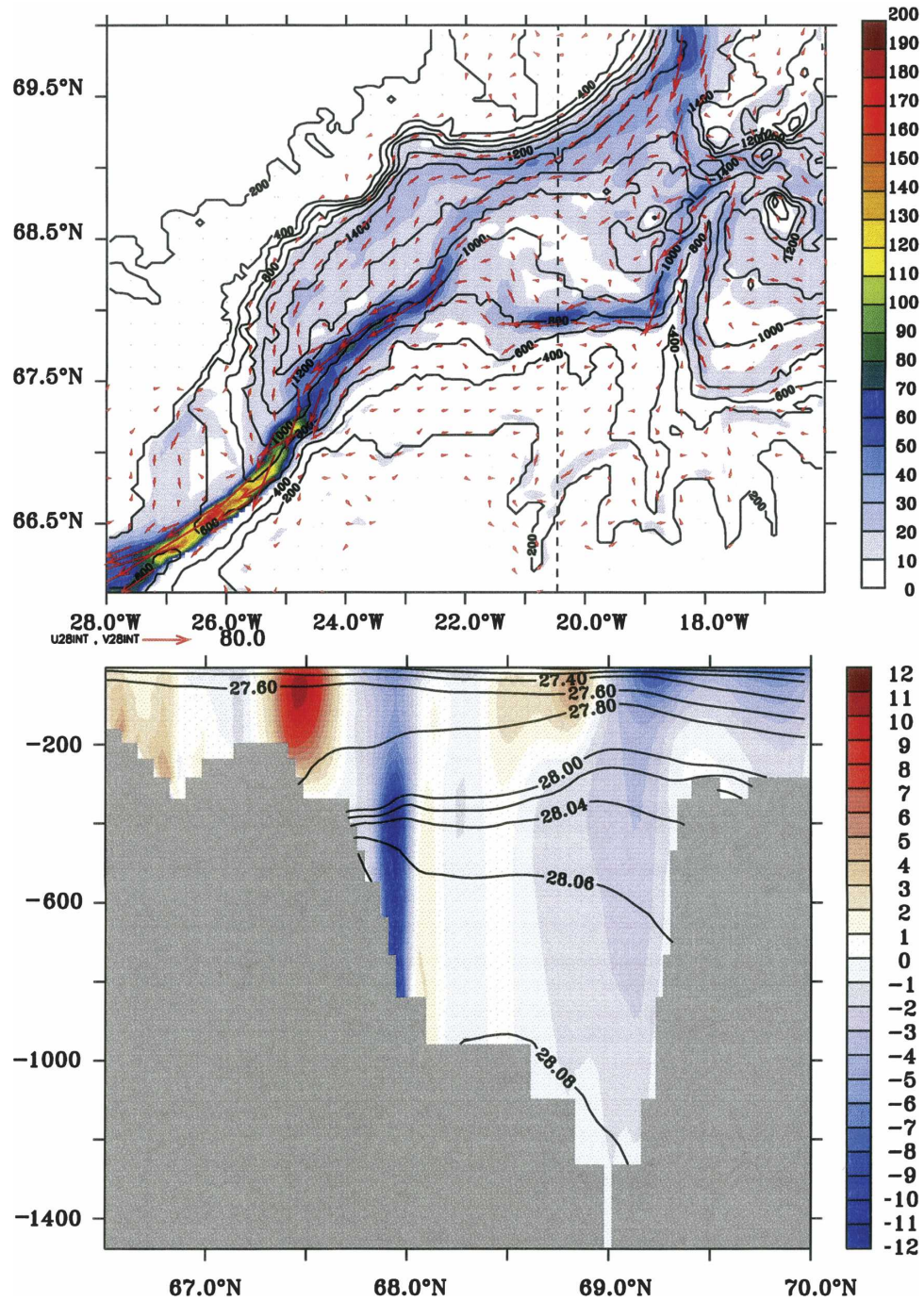
FIG. 3. (top) Mean volume transport densities ($m^2\,s^{-1}$) below the depth of the density surface $\sigma_0 =$ 27.8 averaged over 1993–96. The figure indicates two source regions of the DSOW north of Iceland associated with a branch flowing north of Iceland and the EGC, respectively. Contour increment is $10\,m^2\,s^{-1}$, and the reference velocity vector in the lower left corner represents $80\,m^2\,s^{-1}$. (bottom) Zonal velocities (contour increment $1\,cm\,s^{-1}$) and σ_0 contours plotted along the Hornbanki section at 20.5°W, marked as a dashed line in the top panel.
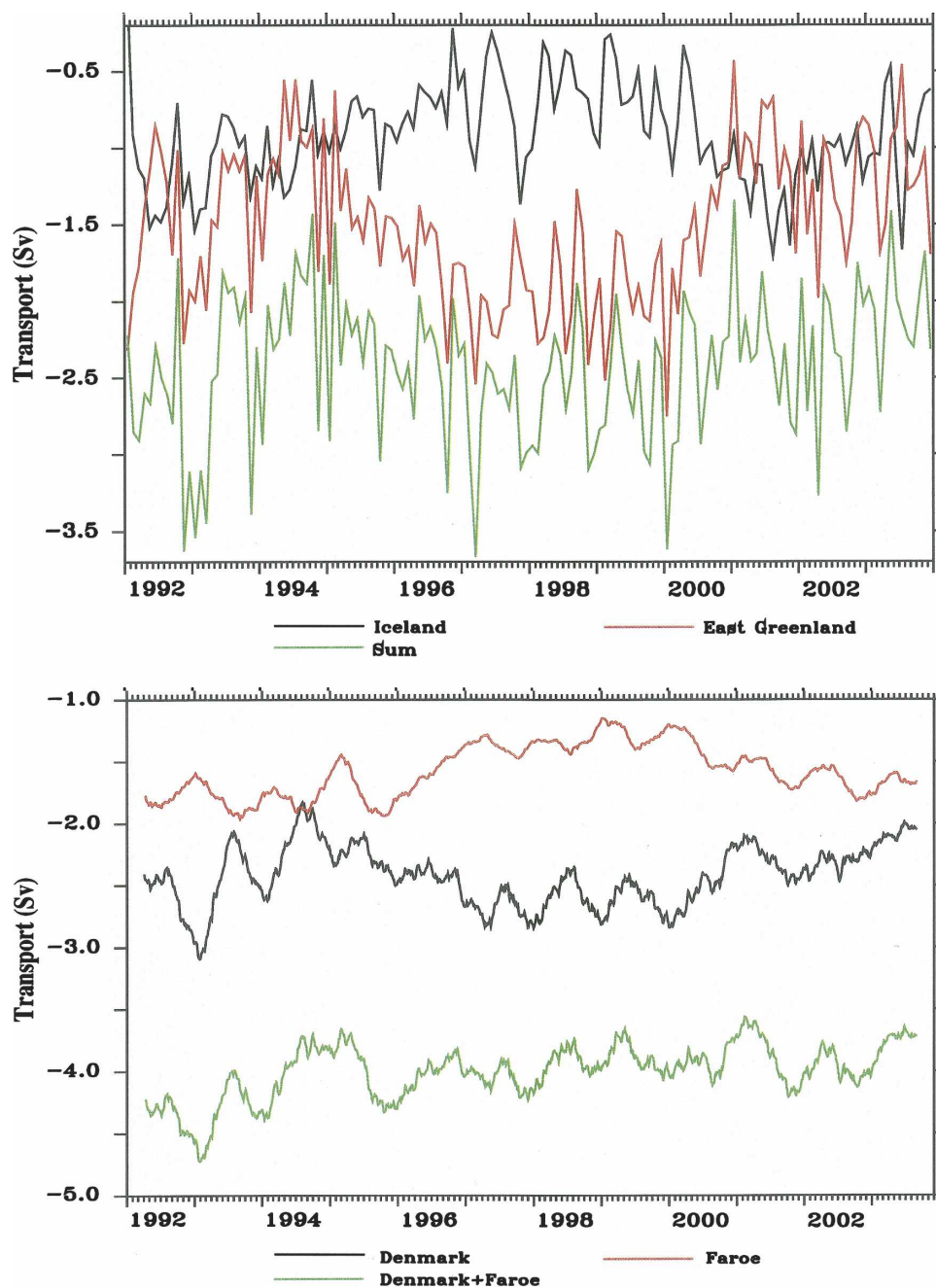
FIG. 4. (top) Time series of monthly mean transports calculated below the depth of the density surface $\sigma_0 = 27.8$ (Sv; positive values are eastward) across the meridional section at 20.5°W shown in Fig. 3. The black and red curves are associated with the branch north of Iceland (67.5°–68.1°N) and the EGC (68.1°–70°N) visible in the top panel of Fig. 3. The black curve shows the sum of both transport time series. (bottom) Net volume transports computed below the depth of the density surface $\sigma_0 = 27.8$ east (Faroe Bank, 58°–62°N, 7°W, red) and west (Denmark Strait, 66°–70°N, 25°W, black) of Iceland. Each curve was filtered with a 183-day running-mean window; positive values are eastward. The net dense transport across the GISR is shown as a green curve. Transports through Denmark Strait and Faroe Bank are negatively correlated with $r = 0.53$.
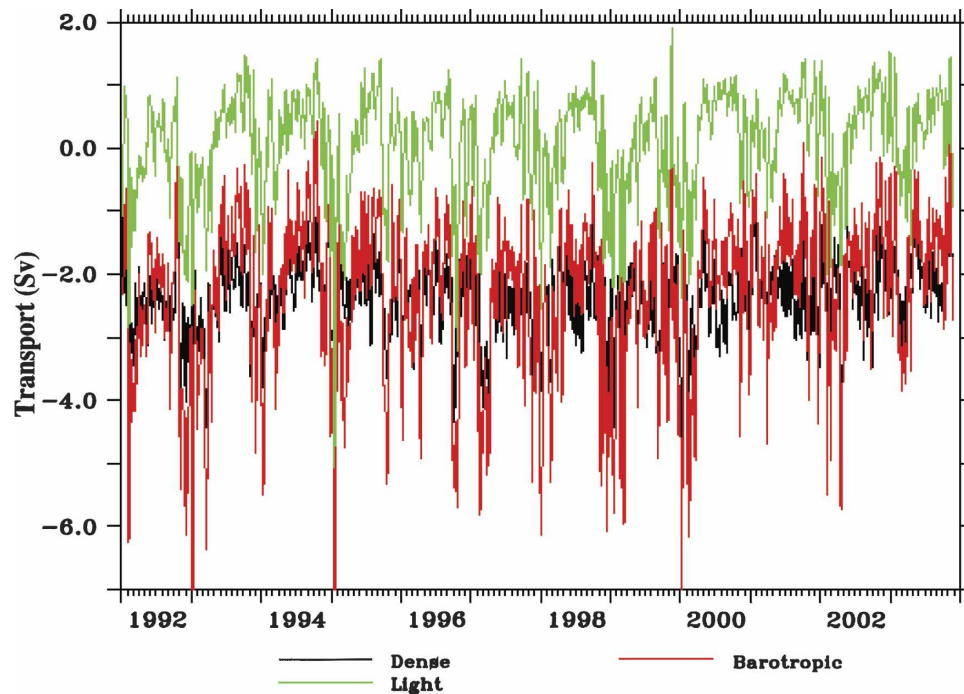
FIG. 5. Volume transports (Sv) through the Denmark Straight computed along 25°W between 67.5° and 68.1°N above and below the density surface $\sigma_0 = 27.8$ for dense (black) and light (green) water and total barotropic transport (red). Each curve was filtered with a 9-day running-mean window for clarity of the plot. The correlation coefficient between the dense and barotropic flows is 0.8 for the filtered and unfiltered time series.

port. The high variability of the barotropic transport is associated with the flow field on the shelf indicated in Fig. 4. Measurement programs aiming at monitoring Denmark Strait (DS) transport changes therefore should also cover the shelf regions. Note that there is no net transport associated with the light part of the flow because the south and northward flowing contributions on either side of DS balance in the model.

4. Mechanisms for DS transport variations

The previous section has illustrated the amount of variability in the DSO and its feeding currents simulated and observed. We will now attempt to describe the underlying physical principles. Our focus will be on the mechanisms occurring in the direct vicinity of the DS ridge. Possible remote mechanisms that can explain the variability of the feeding current north east of Iceland are provided by R. Käse et al. (2006, unpublished manuscript).

For a hydraulic control of the outflow over the Denmark Strait sill the theory of Whitehead (1998) predicts the upper limit for the transport (over a rectangular sill with width much wider than a Rossby radius) to be

$$V_{max} = \frac{1}{2} \frac{g}{f} \frac{\Delta\rho}{\rho} H^2. \tag{1}$$

Here g is the gravity, f is the Coriolis parameter, ρ is the density, and $\Delta\rho$ is the density contrast between lower and upper layer (for a two-layer model) or across the sill; H is the reservoir height above the sill measured upstream. Whitehead's formula corresponds to the difference in potential energy across the sill divided by f. Several approaches to estimate the reservoir height H can be thought of. One obvious choice is to establish a relation between outflow and the maximum height of the $\sigma_0 = 27.8$ surface, h_{eff}.

In the presence of eddy noise, integral quantities are usually a better estimator. We therefore provide here the following estimate of H, which is defined by 2 times the depth of the center of mass of dense water, weighted by the zonal velocity as

$$z_{eff}(x) = \frac{\int_{-H}^{z(\sigma=27.8)} \int_{66}^{71} zu \, dy \, dz}{\int_{-H}^{z(\sigma=27.8)} \int_{66}^{71} u \, dy \, dz}. \tag{2}$$

Multiplied by the area below $\sigma_0 = 27.8$, z_{eff} directly measures the potential energy of the source water.

With $\Delta\rho = 0.34$ kg m^{-3} measured as the density difference (averaged over the height above the sill, 0–590 m) across the sill, the overflow transport can now be

predicted from either h_{eff} or 2 times z_{eff} according to the Whitehead relation. The mean predicted overflow is then 0.91 and 0.64 times the maximum transport (1), respectively, which only for the latter case comes close to the factor of 9/16 that Stern (2004) found for a parabolic bottom profile from a different theoretical consideration. The strong dependence of the time-mean transport estimate on the definition of the reservoir height shows that the estimation of transports via (1) is problematic in continuously stratified conditions and thus requires an empirically estimated factor of proportionality.

An alternative relation describing the upper limit for transports is provided by Helfrich and Pratt (2003) who explored the validity of the Gill (1977) model. They found that the circulation farther upstream is not controlled by the sill. This conclusion is reassuring because it enables the determination of the transport from measurements at the entrance of the sill. In fact, they demonstrated that (1) gives a reasonable approximation to the actual transport if the interface height is taken from the right-hand wall in the entrance region rather than in the center of the upstream basin. Although (1) could be obtained through geostrophic calculation under special preconditions, Helfrich and Pratt (2003) give a slightly more general expression of the transport through a rectangular channel assuming geostrophy:

$$V_{max} = 2\frac{g}{f}\frac{\Delta\rho}{\rho}\hat{h}\bar{h}, \quad (3)$$

$$\hat{h} = (1/2)(h_R - h_L), \quad \text{and} \quad (4)$$

$$\bar{h} = (1/2)(h_R + h_L), \quad (5)$$

where h_R and h_L are the depth of the interface on the right and left walls of the channel, respectively.

For a prediction of V_{max} according to (3) we note that with h_L chosen to be the height of the sill, (3) transforms into (1) and for any larger h_L the transport is reduced by $g/(2f) \times \Delta\rho/\rho h_L^2$. To determine h_R and h_L, maximum and minimum height of the $\sigma_0 = 27.8$ surface are considered. With this definition, h_L is nearly constant at 164 m above the sill (see also Fig. 8 for the location of the $\sigma_0 = 27.8$ contour), which means that the isopycnal slope and thus the geostrophic transport is perfectly correlated with the interface height. In summary, the predicted transport according to (3) differs to the prediction according to Whitehead (1998) only by a constant offset and result in a smaller mean transport of 1.3 Sv because h_L is 164 m above the sill, but shows the same time variability (not shown).

The overflow time series reconstructed from h_{eff} and z_{eff}, both evaluated at 26°W, according to (1) as well as the model overflow are shown in Fig. 6 after applying a 30-day running-mean filter. The standard deviation of the predicted transport is 0.47 Sv for z_{eff} and 0.39 Sv for h_{eff} as compared with 0.41 Sv of the true transport in the model. The prediction based on h_{eff} underestimates variability on time scales shorter than a year whereas the prediction based on z_{eff} shows larger variability than the model transport. The correlation for monthly mean values is $r = 0.40$ for h_{eff} and $r = 0.42$ for z_{eff} but increases to $r = 0.82$ for both, after filtering with an annual window. This is in agreement with the coherence spectrum between h_{eff} or z_{eff} and the dense DSO, as shown in the inset of Fig. 6. The coherence values are significant for periods longer than about a year, demonstrating a close relation between changes in the interface height and the transport variations on those periods. The correlations remain nearly constant for the whole covering area near the entrance of the sill until 25.5°W.

In strict terms, the Whitehead maximum transport theory provides only the time-mean transport and several restrictions apply if used in our case, such as nonstationarity and a complex bottom topography, including a sloping bottom, which, according to Stern (2004), may lead to smaller than maximum estimates. We conclude here from the results shown in Fig. 6 that such a relation is also applicable to the time-varying flow field if transport variations occur on time scales longer than the local synoptic time scale, that is, longer than the order of a week.

To investigate the role of barotropic currents in modifying the DSO, we proceed with a regression of the model DSO time series on the wind stress curl over the subpolar gyre. As shown in Fig. 7, a large correlation between changes in DSO and the local wind stress is found mainly around Iceland. It has been shown previously (Käse et al. 2003) that the contribution of the *observed* barotropic component to the DSO is larger than 70%, which compares with 93% in our simulation. We also found a significant correlation and good skill in the reconstruction of the DSO from the barotropic transport (see Fig. 5) and therefore expect the high correlation with the wind stress curl. The lower panel of Fig. 7 shows the reconstruction of DSO from the wind stress curl averaged over 61°–73°N and 38°–10°W (with positive sign for transfer of momentum into the atmosphere). For monthly mean values, the correlation coefficient with the barotropic transport is $r = 0.72$ and to the dense DSO is $r = 0.57$.

The link between wind stress curl and the barotropic transport is represented by the barotropic vorticity equation, and the resulting Sverdrup balance in the presence of islands is, in its simplest configuration, de-
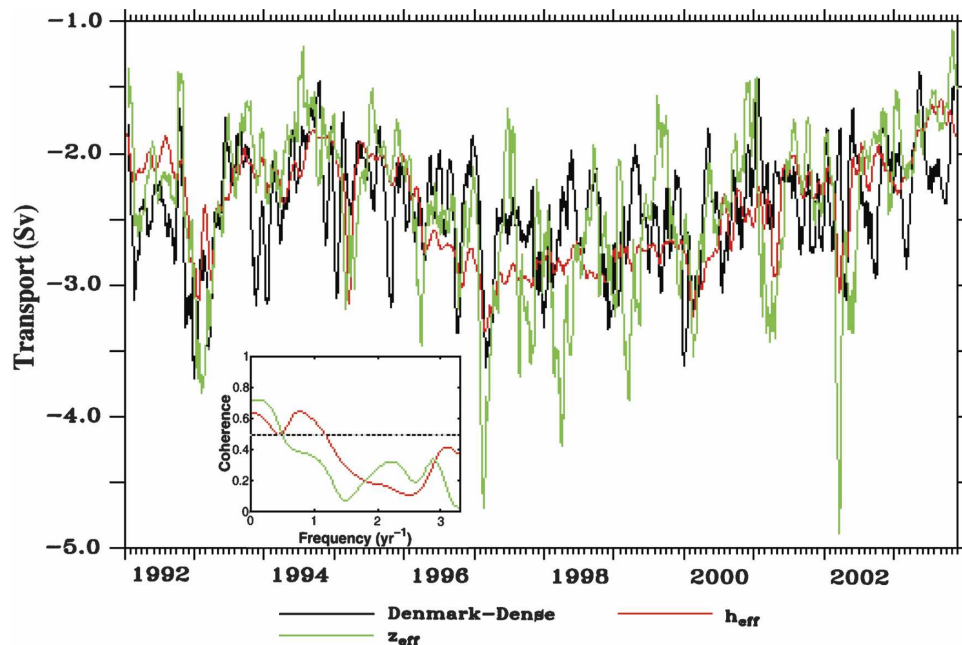
FIG. 6. Dense (below the density surface $\sigma_0 = 27.8$) transport through the Denmark Strait (66°–70°N, 25°W) (black), and transport reconstructions from the interface height z_{eff} (green) and h_{eff} (red) at 26°W based on (1). All curves were filtered with a 30-day running-mean window. The inset shows the coherence spectrum between the overflow and z_{eff} (green) and h_{eff} (red), respectively. The dotted line indicates the 95% significance level from correlation with white noise.

scribed by the *island rule* (Godfrey 1989). However, several restrictions apply in the presence of neglected friction and extreme topographic interactions. Especially in high latitudes topographic interactions become more and more dominant. Pratt and Pedlosky (1998), for instance, describe modifications to the original island rule to account for strong frictional effects that lead to the overestimation of transports by the original rule and also address the application for the transport through Denmark Strait. In agreement with Pratt and Pedlosky (1998), we find a substantial overestimation of the mean transport when applying the original island rule to estimates of the barotropic transport through Denmark Strait. Yet the result shows very good correlation with the barotropic transport and with the DSO with coefficients of $r = 0.79$ and $r = 0.63$, respectively. However, a correct estimation of the transport that takes topography and friction into account appears to be extremely difficult in our application (especially the calculation of the topographic effect is numerically too inaccurate).

The DSO contains a significant barotropic signal (93%), which is much less for the flow through Shetland Channel (33%). In summary, we find that the barotropic flow through Denmark Strait, driven by the wind stress curl, changes the overflow and that the significant correlations of the overflow with wind stress ($r = 0.57$)

can be regarded as an indirect effect. However, the increased barotropic transport also carries more dense water toward the entrance of the Denmark Strait, which again raises the reservoir height until the increased overflow compensates this effect. The combined effect is shown in Fig. 8 for the low-transport case in 1994 (red) and high-transport case in 1999 (blue). The figure shows a higher slope as well as a thicker layer of dense water in 1999. Since an enhancement of the flow through Denmark Strait is associated with a reduced flow through Shetland Channel, this mechanism is also consistent with the anticorrelation between DS and FB overflow variability.

The interpretation of the overflow as a mere consequence of the barotropic transport and ultimately the wind stress curl seems to be neither complete. A closer look at the time scales for which significant correlations exist between DSO and barotropic transport changes makes this point more clear. The inset of Fig. 7 shows that the coherence between wind stress curl and barotropic transport drops off on time scales longer than two years, which is even more noticeable for the coherence between wind stress curl and the overflow. In contrast to this, the coherence between overflow and barotropic transport as shown in the inset of Fig. 7 shows a slight increase on these time scales. The inset of Fig. 6 shows that a large coherence between the reservoir
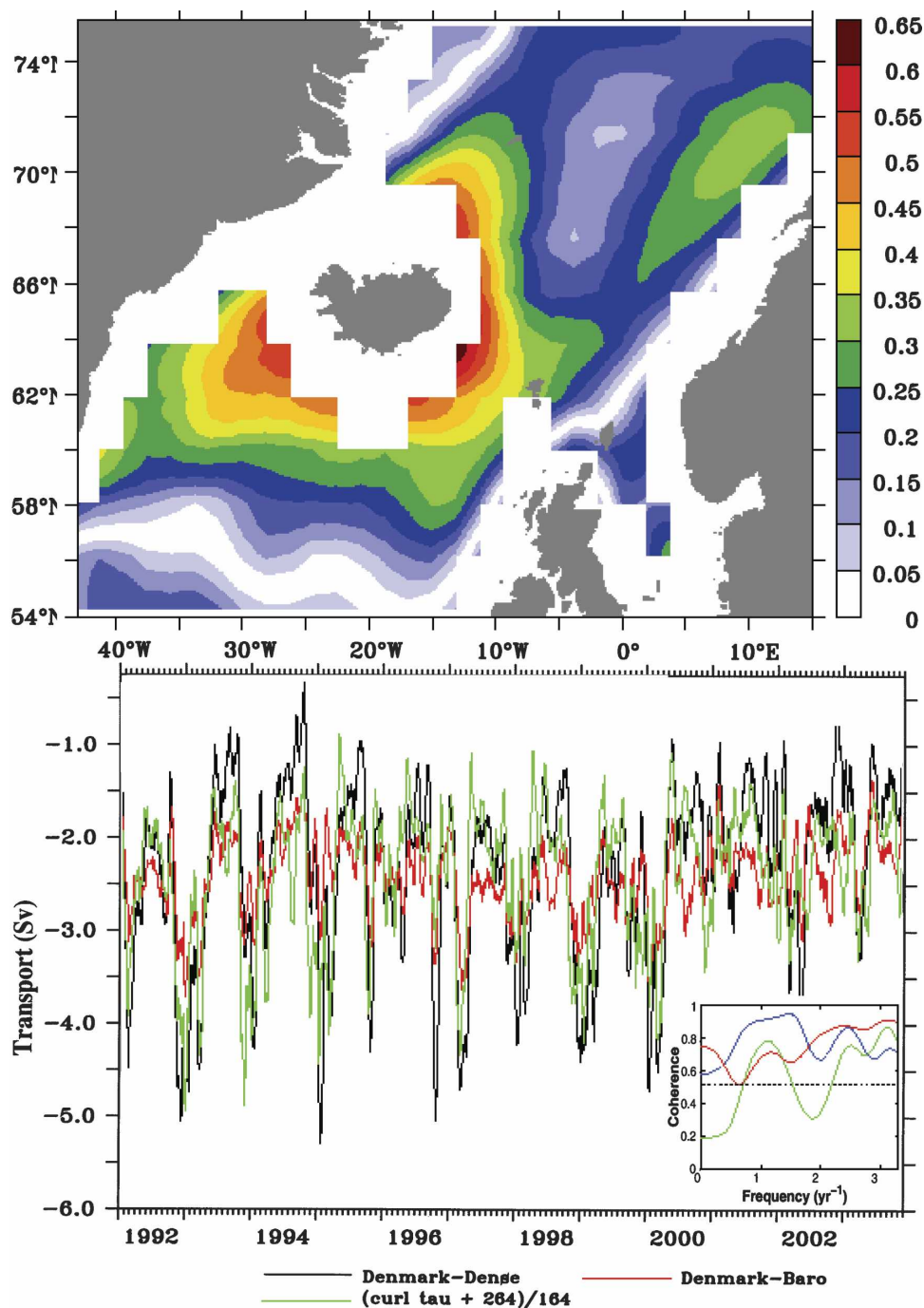
FIG. 7. (top) Correlation coefficient of the regression between monthly mean barotropic transport through Denmark Strait and wind stress curl (curl τ) calculated on the original NCEP grid (white areas are due to differentiation). (bottom) Monthly mean barotropic (black) and dense Denmark Strait (red) transports (Sv) and regression curl τ (N km^{-3}) (green) averaged over 61°–73°N and 38°–5°W. Shown is the regression on the dense Denmark Strait transport ($r = 0.57$). The correlation coefficient with the barotropic transport is $r = 0.73$. All time series were filtered with a 30-day window. The inset shows the coherence between overflow and wind stress curl (green), the overflow and barotropic transport (red), and the wind stress curl and barotropic transport (blue), respectively. The dotted line indicates the 95% significance level from correlation with white noise.
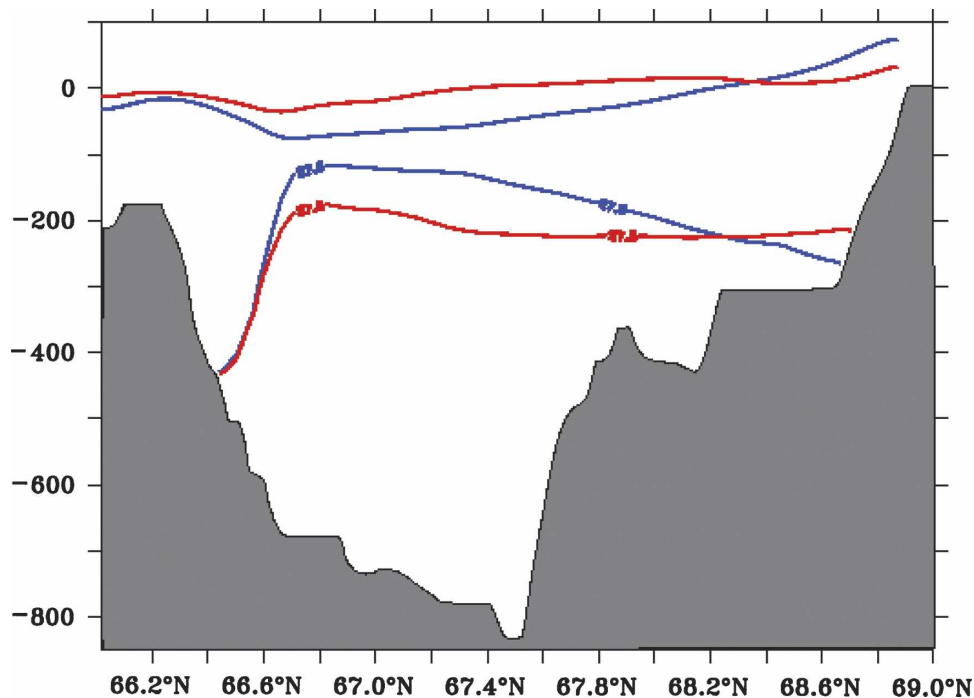
FIG. 8. Relation between changes in SSH ($\times 1000$) and $\sigma_0 = 27.8$ surfaces for low transports in 1994 (red) and high transports in 1999 (blue).

height (measured by z_{eff} or h_{eff}) and the overflow exists only on time scales longer than a year. This indicates that on long time scales the barotropic transport across the DS sill is actually determined by the overflow and not vice versa. On these long time scales the amount of dense water that is carried by the two branches shown in Fig. 4 toward the entrance of the Denmark Strait is dominant for determining the transports.

On long time scales, the variability and anticorrelation of the transport time series of the two branches corresponds well with variability and anticorrelation of the time series of the DSO and FBO (Fig. 4). To explain the connection of the local correlation of the two branches at the entrance of the Denmark Strait to the correlation over a longer distance between DSO and FBO, variability of different sources of dense water have to be considered (R. Käse et al. 2006, unpublished manuscript).

5. Observability of DSO

The above result suggests that estimates such as h_{eff} can be used as a proxy to monitor transport variations of the DSO. However, h_{eff} and especially z_{eff} are difficult to monitor, and a relation to quantities that are remotely measurable such as sea surface height (SSH) would be preferable (from the discussion above we

have already revealed the potential of wind stress measurements for the determination of DSO changes). The possibility to detect subsurface water mass changes from altimeter data was already suggested by Stammer et al. (1991) who showed the detectability of Mediterranean outflow eddies from *Geosat* data. To investigate this possibility we show in Fig. 9 a schematic of the interplay of SSH variability and the level of dense water as described by its center z_{eff}. In its upper panel, the figure shows z_{eff} together with the minimum SSH between 66° and 70°N for 1994 and 1999, which represent low- and high-transport years, respectively. Accordingly, a depression of the sea level indicates a higher-than-normal thickness of dense water and vice versa. In its lower panel, Fig. 9 shows the scaled time series of minimum SSH along 25°W together with time series of z_{eff} (for an easier comparison with the upper panel, z_{eff} was measured in this figure from the surface). The scaling factor of about 1000 determined from a regression implies that 1-cm change of ΔSSH corresponds to 10-m fluctuation in reservoir height. The correlation between both time series is 0.6. In both time series we find variations on intraseasonal time scale superimposed to multiyear changes; in particular we find significantly lower SSH and z_{eff} values during 1996–2000.

A geographical distribution of the correlation coefficients of a regression between time series of DSO and

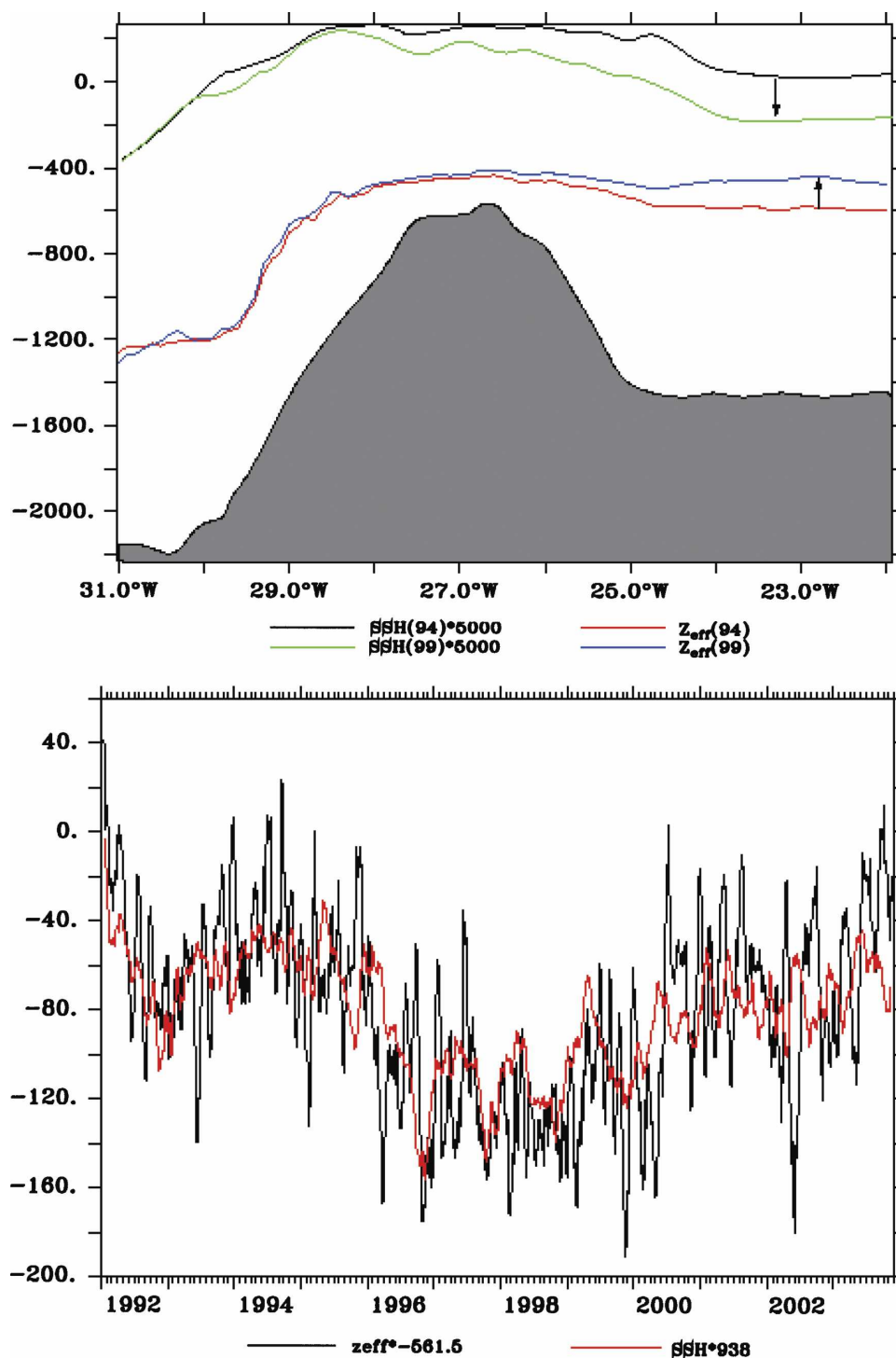FIG. 9. (top) Interplay between the center of dense water, z_{eff}, and the minimum SSH level both diagnosed from annual mean model fields between 66° and 70°N for the low transport and high transport phased during 1994 (SSH, black; z_{eff}, red) and 1999 (SSH, green; z_{eff}, blue), respectively. In the figure, the SSH values were multiplied by a factor of 5000. The topography is the maximum depth between 66° and 70°N, which in general does not coincide with the location of the minimum SSH. (bottom) Time series of the depth of z_{eff} (black) and the minimum SSH along 25°W (red) including parameters from the regression of z_{eff} against SSH. The time series of z_{eff} is plotted as the difference to the intercept 561.5 m and the difference is very close to the height above the sill depth of the model (−590 m). The SSH time series is scaled with the slope (938). Both series were filtered with a 30-day running-mean window, and the correlation coefficient between them is $r = 0.60$. Using a 1-yr running-mean filter, the correlation increases to $r = 0.97$ but is only 0.14 if based on unfiltered time series. Values are provided in meters.

SSH (after filtering with a 30-day window) is provided in the top panel of Fig. 10. There are high correlation values downstream of the Denmark Strait and northeast of it. The detectability of the downstream fluctuation by altimeter data was described by Hoyer and Quadfasel (2001). The correlation between DSO and the SSH downstream is slightly larger for a lag of 1–2 months (DSO leading). This part of the correlation is thus greatly reduced if the plot were based on the snapshot values. This is in accord with the findings of Köhl and Stammer (2004) who describe the downstream SSH as the optimal place to hindcast DSO variability with a few months lag.

Upstream of the DSO, negative coefficients are located along the coast lines and positive coefficients can be found in the center of the Nordic seas with especially high values near the entrance of the strait. In its bottom panel, the figure shows a scatterplot based on the snapshot values of the DSO together with SSH time series, the latter taken slightly upstream of the overflow at the position (66.5°N, 25.3°W). The scaling factor is 0.24 Sv cm^{-1}, and the regression coefficient is 0.84. Note that the southward transport is negative. Thus large transport values are associated locally with a depression of the SSH and remotely with an intensification of the cyclonic circulation in the GIN Sea, meaning stronger North Atlantic inflow and a stronger EGC.

The barotropic transport variability can also be derived from SSH gradients, assuming that the transport variability is predominantly barotropic and represented by the geostrophic surface current and thus the SSH slope. Then the relation between the barotropic transport across 66°N and the sea surface height ζ reads

$$V_{\text{baro}} = -\int_{36W}^{24W} \frac{gH}{f} \frac{\partial \zeta}{\partial x} \, dx. \tag{6}$$

The scatterplot in Fig. 10 shows the regression of the geostrophic transport according to (6) and the barotropic transport for monthly mean values. The resulting time-mean transport is with 1.3 Sv only about one-half of the barotropic transport that is to be expected since the overflow is bottom intensified and inflow of Atlantic water exists at shallow depth. The correlation is high ($r = 0.87$), which confirms the assumption that the transport variability can be described to first order by a barotropic flow. Because of the correlation between barotropic transport and overflow, a high correlation ($r = 0.68$) also exists between the overflow and the geostrophic transport.

In summary, we find a close agreement of the transport variations of dense water with large scale as well as local changes. We conclude that in principle altimetric

satellite observations of SSH should be appropriate to monitor changes in the Denmark Strait transport. To what extent this holds for real observations is investigated now by applying our results to the altimetric sea level along track data from the Ocean Topography Experiment (TOPEX), *Jason-1*, *Environmental Research Satellite-2* (*ERS-2*), and the *Environmental Satellite* (*ENVISAT*). On interannual time scales more than 50% of the SSH variability is due to a large-scale signal that seems to include a substantial thermosteric fraction due to the warming of the Nordic seas. Moreover, the basin mean was found to be nearly identical to the mean south of 66°N, which indicates that the large-scale SSH north of 66°N (exclusively measured by *ERS-2* and *ENVISAT*) is not independent of the SSH south of 66°N where TOPEX and *Jason-1* are available. The result of the predictions after removing the basin mean of TOPEX/*Jason-1* and *ERS-2*/*ENVISAT* SSH, which should not contain implications for the DSO and which are for instance not simulated by the model, is shown in Fig. 11 (red and black curve). A comparison of the prediction based on TOPEX/*Jason-1* and on *ERS-2*/*ENVISAT* data reveals some insight into estimation uncertainties due to uncertainties in the SSH observations. Some of the short-term variability of the SSH-derived transports seems not to be reliable since it depends on the satellite mission whereas the long-term tendencies show good agreement. Based on the regression shown in Fig. 10 it follows that a 1-cm SSH error corresponds to a 0.14-Sv transport error. An rms difference of 1.3 cm (corresponding to 0.18 Sv) between the two different SSH data sources was found for the data used in the figure, which is considerably smaller than the estimation of the pointwise measurement error of about 4 cm (e.g., Chelton et al. 2001).

Also shown in this figure are two further recent estimates of the DSO variability that allow an independent evaluation of the SSH-based prediction (all series are filtered consistently with a 3-month running mean and the mean values are removed for easier comparison). The time series based on ADCP measurements upstream of the sill [A. Macrander 2005, personal communication; see also Macrander et al. (2005); green line] shows a decline of the transports by about 0.6 Sv after about 2000. An additional time series recorded in a current-meter array downstream of the sill at Angmagssalik, Greenland (AWI-Bremerhaven 2006, kindly provided by S. Dye, R. Dickson, and J. Meincke), shows an increase until mid-2000 and a decrease thereafter. A short time lag (the upstream transport leading by 70 days) between these two estimates is discussed by AWI-Bremerhaven (2006) and is consistent with the propagation speed of the signal given the
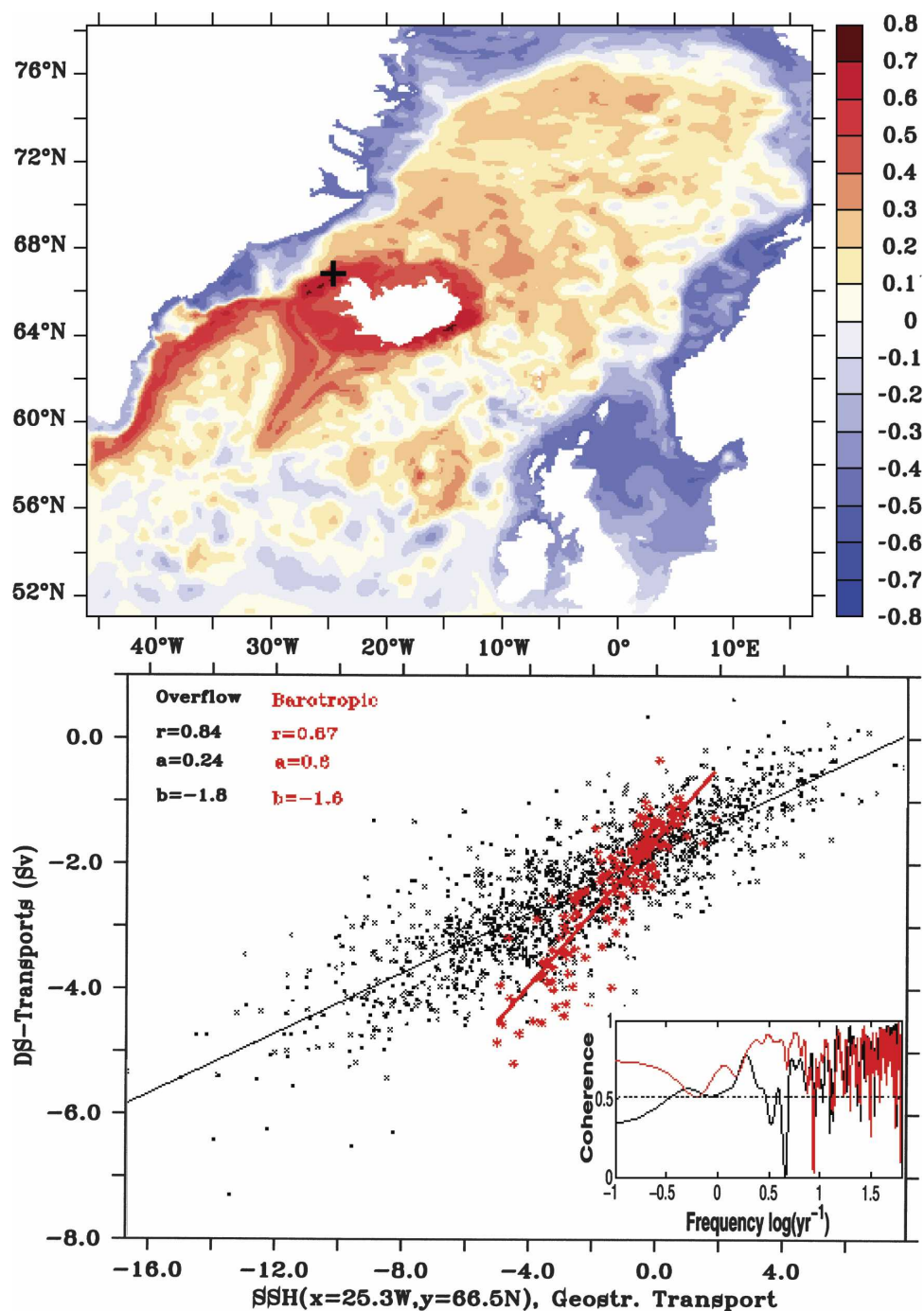
FIG. 10. (top) Correlation coefficient of the regression between time series of Denmark Strait transport and SSH filtered with a 30-day running-mean window. (bottom) Scatterplot of the unfiltered Denmark Strait transport and SSH in centimeters at the location (66.5°N, 25.3°W, marked by the cross in the top panel) (black) and of monthly mean values of the barotropic transport and the geostrophic transport according to (6) (red). The inset shows the coherence spectrum between the DSO and SSH at (66.5°N, 25.3°W) (black) as well as the coherence between the barotropic and geostrophic transports (red). The dotted line indicates the 95% significance level from correlation with white noise.
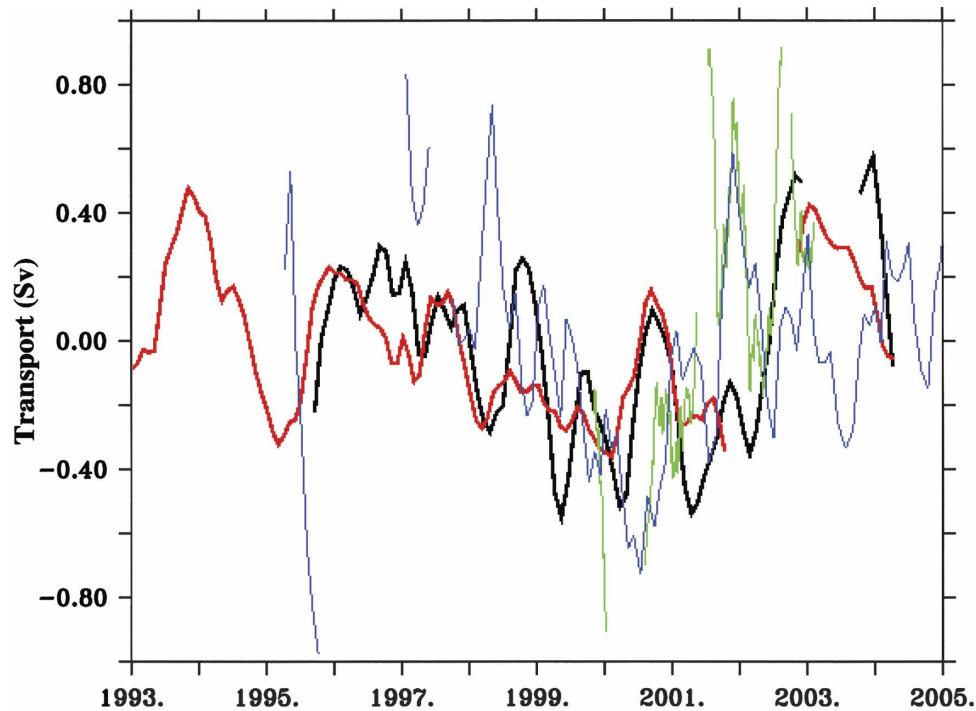
FIG. 11. Estimates of DSO based on ADCP data provided by Macrander et al. (2005) (green) and based on current-meter data provided by AWI-Bremerhaven (2006) (blue), plotted together with transports predicted by this study from along-track SSH data averaged over 66°–67°N, 26°–25°W with their basin mean removed. Red and black curves represent respective results from TOPEX/*Jason-1* and *ERS-1/ENVISAT*, respectively. Transports are in Sverdrups, the time mean is removed from each curve, and all curves were filtered with a 3-month running-mean window as done by Macrander et al. (2005).

distance. The general tendencies (increase until 2000–01 and decrease thereafter) are consistent with all estimates and gives confidence in the capability of the altimeter-based method. As expected, the short-term variability of the SSH-derived transports is considerably different from the current-meter estimates, which considerably differ among each other on these time scales. For a final assessment of this possibility to predict the DSO from remote sensing data a longer times series of in situ measurements is required.

6. Discussion and concluding remarks

The paper focuses on simulating the variability of the circulation in the Nordic seas to give insight into mechanisms that may lead to changes of the transport of dense water through Denmark Strait. Here we have to note that, although the model was driven with the atmospheric state of 1992–2003 and simulates some aspects of the circulation during this period realistically, deficiencies concerning the boundary and initial conditions limit the skill of our solution and restrict the comparison with observational data. In particular, the time-mean transport of the DSO is 2.4 Sv in the model and thus lower than estimations based on recent observations [3.1–3.7 Sv reported by Macrander et al. (2005)]. However, observations are based on measurements much closer to the sill, and the model results indicate that at this position the observed overflow transport contains already at least 0.3-Sv entrained water.

The current flowing north of Iceland toward the Denmark Strait discovered by Jónsson and Valdimarsson (2004) is reproduced by the model, which additionally reveals that the current is part of a two-branch system that includes the EGC as the second branch. It is shown here from the model results that the system is highly variable on all time scales and that transport estimations based on short-term measurements are prone to large errors. The Icelandic branch may carry nearly one-half of the transport of the DSOW but may at other times only account for less the 20% of the transport. On time scales longer than one year, the variability of the two-branch system is anticorrelated and seems to reflect the variability of the system consisting of FBO and DSO. The relation between these two systems was not the focus of the present article. Because of

their anticorrelation, the total transport of dense water through FBO and DSO is found to be constant over the simulated period, which stands in contrast to the findings of Bacon (1998) who found substantial variability of the overflows if measured farther downstream east of Cape Farewell.

We use the fact that the overflow through Denmark Strait is hydraulically controlled in order to apply a relation between DSO variability and changes in the upstream basin, which finally is used to propose a simple system for monitoring the transport variability. In specific terms, a connection between interface height and sea surface height is established, which enables monitoring of the overflow through altimetry. The classical theories of Whitehead (1998) and Helfrich and Pratt (2003) that describe the maximum transport over a sill in a steady situation are tested with the time-varying flow. We found, on time scales much longer than the synoptic time scale, both theories to be also consistent with the time-varying transports. The transport can thus be inferred purely from measuring the upstream interface height. However, on time scales shorter than a few months the relation to the interface height is lost.

The barotropic transport variability can be diagnosed from the geostrophic surface currents and thus from the slope of the sea surface height. The DSO can be estimated from the SSH signature of reservoir height changes. To be able to monitor small long-term transport changes from altimeter, high accuracy is required; 1-cm SSH uncertainty corresponds to 0.14-Sv transport. Results from different altimeter products agree well and indicate that the accuracy is in fact adequate for monitoring long-term changes. An estimate based entirely on altimeter measurements of SSH reproduces recent results of Macrander et al. (2005) and AWI-Bremerhaven (2006) that the DSO has increased until 2000 and decreased thereafter. The agreement provides confidence for all of the estimations on longer time scales. The short-term variability depends on the satellite mission and is also different for the two current-meter-based measurements.

Shorter-term changes of the overflow are found to be mainly concurrent with the variability of the barotropic transport. The large barotropic component of the overflow (more than 90% in the model) masks causalities. We suggest that the barotropic transport is wind driven, and the wind stress curl around Iceland the most important factor in determining the transport. The good correlation of the overflow with the wind stress curl is thus mainly due to this indirect mechanism, which becomes less effective on longer time scales. Although the simple island rule (Godfrey 1989) overestimates the barotropic transport considerably, the excellent correlation to the transport indicates that modifications (especially including topographic effects) to the original rule may be able to correct for this. On the long time scales hydraulic control is the dominant mechanism determining the DSO, but enhanced DSO will also affect the barotropic transport. There is also an effect of the barotropic transport on the DSO on long time scales such as that the barotropic transport carries also more dense water toward the sill, which will enhance the reservoir high near the entrance.

In this study we focused on direct correlation between DSO and various proxies. Orvik and Skagseth (2003), however, presented a relation of the Norwegian Slope Current to remote wind stress curl changes. They found a 15-month lag between the wind stress data and the transport of the current, which they explain as a forced baroclinic Rossby wave response to the remote wind forcing. The investigation of lags between DSO and remote wind stress curl from our simulation revealed no significant correlations. Only the before-mentioned lags of a few months between SSH and DSO are found to be significant.

REFERENCES

AWI-Bremerhaven, 2006: Arctic-Subarctic Ocean Flux Array for European Climate: West (ASOF-W). Final Scientific Report, 162 pp.

Bacon, S., 1998: Decadal variability in the outflow from the Nordic seas to the deep Atlantic Ocean. *Nature,* **394,** 871–874.

Biastoch, A., R. Käse, and D. Stammer, 2003: The sensitivity of the Greenland–Scotland Ridge overflow to forcing changes. *J. Phys. Oceanogr.,* **33,** 2307–2319.

Borenäs, K., and P. Lundberg, 2004: The Faroe-Bank Channel deep-water overflow. *Deep-Sea Res. II,* **4–5,** 335–350.

Chelton, D. B., J. Ries, B. Haines, L.-L. Fu, and P. Callahan, 2001: Satellite altimetry. *Satellite Altimetry and Earth Sciences,* L.-L. Fu and A. Cazenave, Eds., Academic Press, 1–131.

Dickson, B., J. Meincke, I. Vassie, J. Jungclaus, and S. Østerhus, 1999: Possible predictability in overflow from the Denmark Strait. *Nature,* **397,** 243–246.

Dickson, R. R., and J. Brown, 1994: The production of North Atlantic deep water: Sources, rates and pathways. *J. Geophys. Res.,* **99,** 12 319–12 341.

Fahrbach, B. R. E., J. Meincke, G. Budeus, and P. Eriksson, 2002: The East Greenland Current and its contribution to the Denmark Strait overflow. *ICES J. Mar. Sci.,* **59,** 1133–1154.

Gill, A. E., 1977: The hydraulics of rotating-channel flow. *J. Fluid Mech.,* **80,** 641–671.

Girton, J. B., T. B. Sanford, and R. H. Käse, 2001: Synoptic sections of the Denmark Strait overflow. *Geophys. Res. Lett.,* **28,** 1619–1622.

Godfrey, J. S., 1989: A Sverdrup model of the depth-integrated flow from the world ocean allowing for island circulations. *Deep-Sea Res.,* **45,** 89–112.

Hansen, B., W. R. Turrell, and S. Østerhus, 2001: Decreasing overflows from the Nordic seas into the North Atlantic Ocean through the Faroe Bank Channel since 1950. *Nature,* **411,** 927–930.

Helfrich, K. R., and L. J. Pratt, 2003: Rotating hydraulics and upstream basin circulation. *J. Phys. Oceanogr.,* **33,** 1651–1663.

Hoyer, J. L., and D. Quadfasel, 2001: Detection of deep overflows with satellite altimetry. *Geophys. Res. Lett.,* **28,** 1611–1614.

Jerlov, N. G., 1968: *Optical Oceanography.* Elsevier, 199 pp.

Jónsson, S., and H. Valdimarsson, 2004: A new path for the Denmark Strait overflow water from the Iceland Sea to Denmark Strait. *Geophys. Res. Lett.,* **31,** L03305, doi:10.1029/2003GL019214.

Käse, R. H., and A. Oschlies, 2000: Flow through Denmark Strait. *J. Geophys. Res.,* **105,** 28 527–28 546.

——, J. B. Girton, and T. B. Sanford, 2003: Structure and variability of the Denmark Strait overflow: Model and observations. *J. Geophys. Res,* **108,** 3181, doi:10.1029/2002JC001548.

Köhl, A., and D. Stammer, 2004: Optimal observations for variational data assimilation. *J. Phys. Oceanogr.,* **34,** 529–542.

——, ——, and B. Cornuelle, 2007: Interannual to decadal changes in the ECCO global synthesis. *J. Phys. Oceanogr.,* **37,** 313–337.

Kösters, F., R. H. Käse, A. Schmittner, and P. Herrmann, 2005: The effect of Denmark Strait overflow on the Atlantic Meridional Overturning Circulation. *Geophys. Res. Lett.,* **32,** L04602, doi:10.1029/2004GL022112.

Large, W. G., and S. Pond, 1981: Open ocean momentum flux measurements in moderate to strong winds. *J. Phys. Oceanogr.,* **11,** 324–336.

——, and ——, 1982: Sensible and latent-heat flux measurements over the ocean. *J. Phys. Oceanogr.,* **12,** 464–482.

——, J. C. Williams, and S. C. Doney, 1994: Ocean vertical mixing: A review and a model with a nonlocal boundary layer parameterization. *Rev. Geophys.,* **32,** 363–403.

Levitus, S., and T. P. Boyer, 1994: *Temperature.* Vol. 4, *World Ocean Atlas 1994,* NOAA Atlas NESDIS 4, 117 pp.

——, R. Burgett, and T. P. Boyer, 1994: *Salinity.* Vol. 3, *World Ocean Atlas 1994,* NOAA Atlas NESDIS 3, 99 pp.

Macrander, A., U. Send, H. Valdimarsson, S. Jónsson, and R. H. Käse, 2005: Interannual changes in the overflow from the Nordic seas into the Atlantic Ocean through Denmark Strait. *Geophys. Res. Lett.,* **32,** L06606, doi:10.1029/2004GL021463.

Marshall, J., A. Adcroft, C. Hill, L. Perelman, and C. Heisey, 1997a: A finite-volume, incompressible Navier Stokes model for studies of the ocean on parallel computers. *J. Geophys. Res.,* **102,** 5753–5766.

——, C. Hill, L. Perelman, and A. Adcroft, 1997b: Hydrostatic, quasi-hydrostatic, and nonhydrostatic ocean modelling. *J. Geophys. Res.,* **102,** 5733–5752.

Mauritzen, C., 1996a: Production of dense overflow waters feeding the North Atlantic across the Greenland-Scotland Ridge. 1. Evidence for a revised circulation scheme. *Deep-Sea Res. I,* **43,** 769–806.

——, 1996b: Production of dense overflow waters feeding the North Atlantic across the Greenland-Scotland Ridge. 2. An inverse model. *Deep-Sea Res. I,* **43,** 807–835.

——, J. Price, T. Sanford, and D. Torres, 2005: Circulation and mixing in the Faroese Channels. *Deep-Sea Res. I,* **52,** 883–913.

Nilsen, J. E. Ø., Y. Gao, H. Drange, T. Furevik, and M. Bentsen, 2003: Simulated North Atlantic-Nordic seas water mass exchanges in an isopycnic coordinate OGCM. *Geophys. Res. Lett.,* **30,** 1536, doi:10.1029/2002GL016597.

Orvik, K. A., and Ø. Skagseth, 2003: The impact of the wind stress curl in the North Atlantic on the Atlantic inflow to the Norwegian Sea toward the Arctic. *Geophys. Res. Lett.,* **30,** 1884, doi:10.1029/2003GL017932.

Østerhus, S., W. R. Turrell, S. Jónsson, and B. Hansen, 2005: Measured volume, heat, and salt fluxes from the Atlantic to the Arctic Mediterranean. *Geophys. Res. Lett.,* **32,** L07603, doi:10.1029/2004GL022188.

Paulson, C. A., and J. J. Simpson, 1977: Irradiance measurements in the upper ocean. *J. Phys. Oceanogr.,* **7,** 952–956.

Pratt, L., and J. Pedlosky, 1998: Barotropic circulation around islands with friction. *J. Phys. Oceanogr.,* **28,** 2148–2162.

Saunders, P., 2001: The dense northern overflows. *Ocean Circulation and Climate: Observing and Modelling the Global Ocean,* G. Siedler, J. Church, and J. Gould, Eds., Academic Press, 401–417.

Smith, W. H. F., and D. T. Sandwell, 1997: Global seafloor topography from satellite altimetry and ship depth soundings. *Science,* **277,** 195–196.

Stammer, D., H.-H. Hinrichsen, and R. H. Käse, 1991: Can meddies be detected by satellite altimetry? *J. Geophys. Res.,* **96,** 7005–7014.

——, C. Wunsch, I. Fukumori, and J. Marshall, 2002: State estimation improves prospects for ocean research. *Eos, Trans. Amer. Geophys. Union,* **83,** 294–295.

Stern, M. E., 2004: Transport extremum through Denmark Strait. *Geophys. Res. Lett.,* **31,** L12303, doi:10.1029/2004GL020184.

Strass, V. H., E. Fahrbach, U. Schauer, and L. Sellmann, 1993: Formation of Denmark Strait overflow water by mixing in the East Greenland Current. *J. Geophys. Res.,* **98,** 6907–6919.

Swaters, G. E., 1991: On the baroclinic instability of cold-core coupled density fronts on a sloping continental-shelf. *J. Fluid Mech.,* **224,** 361–382.

Wentz, F. J., C. Gentemann, D. Smith, and D. Chelton, 2000: Satellite measurements of sea surface temperature through clouds. *Science,* **288,** 847–850.

Whitehead, P., 1998: Topographic control of oceanic flows in deep passages and straits. *Rev. Geophys.,* **36,** 423–440.

Zhang, J. L., and D. Rothrock, 2000: Modeling Arctic sea ice with an efficient plastic solution. *J. Geophys. Res.,* **105,** 3325–3338.

Zhang, K. Q., and J. Marotzke, 1999: The importance of open-boundary estimation for an Indian Ocean GCM-data synthesis. *J. Mar. Res.,* **57,** 305–334.